ACS Biomaterials SCIENCE & ENGINEERING

pubs.acs.org/journal/abseba
Article

Functionalized Collagen I Membranes as a Bruch's Membrane Mimetic for Outer Retinal *In Vitro* Models

Ashley R. Murphy, Xuen Jen Ng, Grace Lidgerwood, Alice Pébay, Yen B. Truong, Carmel M. O'Brien, and Veronica Glattauer*

Cite This: *ACS Biomater. Sci. Eng.* 2024, 10, 5653−5665
Read Online
ACCESS | Metrics & More | Article Recommendations | Supporting Information

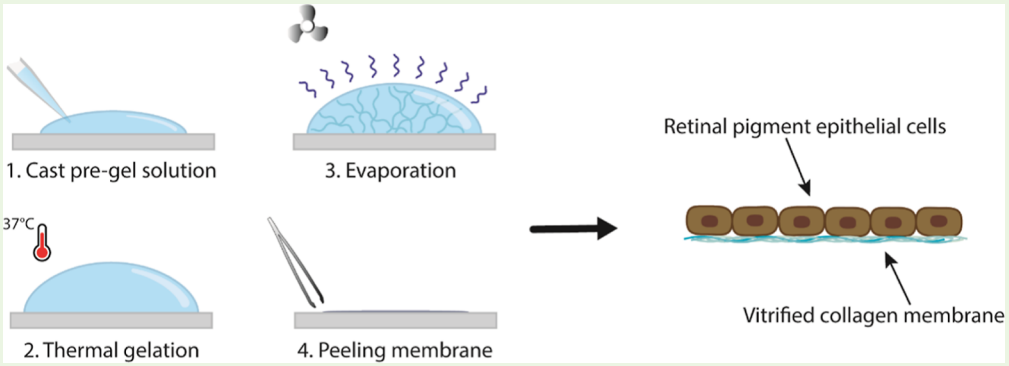

ABSTRACT: Physiologically relevant *in vitro* models of the human outer retina are required to better elucidate the complex interplay of retinal tissue layers and investigate their role in retinal degenerative disorders. Materials currently used to mimic the function of Bruch's membrane fail to replicate a range of important structural, mechanical, and biochemical properties. Here, we detail the fabrication of a surface-functionalized, fibrous collagen I membrane. We demonstrate its ability to better replicate a range of important material properties akin to the function of human Bruch's membrane when compared with a commonly utilized synthetic polyethylene terephthalate alternative. We further reveal the ability of this membrane to support the culture of the ARPE-19 cell line, as well as human pluripotent stem cell-derived RPE-like cells and human umbilical vein endothelial cells. This material could provide greater physiological relevance to the native Bruch's membrane than current synthetic materials and further improve the outcomes of *in vitro* outer retinal models.

KEYWORDS: *Bruch's membrane, retina, retinal pigment epithelium, collagen, in vitro model*

1. INTRODUCTION

Retinal degenerative disorders such as age-related macular degeneration (AMD) and retinitis pigmentosa result in progressive vision loss and are a leading cause of blindness worldwide.[1] Current treatments for these debilitating disorders are only capable of slowing their progression, and therapies to halt or even reverse disease progression long-term currently remain unrealised.[2]

The retina is a multilayered tissue responsible for converting light into a neurological signal that is sent to the brain. The outer retina assists in maintaining the light-converting properties of the retina, and its pathophysiology is commonly associated with retinal degenerative disorders. The outer retina is composed of the retinal pigment epithelium (RPE), a monolayer of pigmented epithelial cells which sits on top of the Bruch's membrane, a thin fibrous material that maintains separation from the choroid, a network of vasculature responsible for biomolecular transport to and from the retina. Dysfunction of these delicate structures commonly leads to vision impairment, and these are often sites for studying retinal degeneration mechanisms.

While animal models are typically utilized to determine the safety and efficacy of experimental retinal therapies, concern remains over the cross-species applicability of these routes of study for retinal degenerative disorders. Holistically, for ethical, financial and time concerns, the medical research field is moving toward the development of *in vitro* models as a means for drug testing, to support a reduced reliance on animal testing.[3] For these reasons, there is a requirement for physiologically accurate human *in vitro* models of the outer

Received: June 18, 2024
Revised: July 30, 2024
Accepted: August 1, 2024
Published: August 12, 2024

https://doi.org/10.1021/acsbiomaterials.4c01112
ACS Biomater. Sci. Eng. 2024, 10, 5653−5665

retina to assist in the accuracy of disease interrogation and high throughput drug discovery studies.

To mimic the native anatomy of the human RPE and Bruch's membrane, *in vitro* models of the outer retina typically employ porous membranes to support the culture of RPE cells. These membranes span a wide range of natural and synthetic materials, including, but not limited to amniotic membrane, collagen I, polylactic acid, parylene-C and polyethylene terephthalate (PET) and have been thoroughly reviewed by the authors.[4] While these materials often provide adequate substrates for supporting a monolayer of viable RPE cells, their relevance to the native human Bruch's membrane, and the influence this imparts on *in vitro* RPE studies, is often poorly defined or completely overlooked.

The native human Bruch's membrane has a unique array of physical and biomolecular properties that are difficult to replicate in totality using common biofabrication techniques.[4] Bruch's membrane is primarily composed of elastin and fibrous collagen and commonly, fibrous collagen membranes are mimicked *via* electrospinning fabrication techniques.[5] However, concern surrounding the denaturing properties of spinning solvents, to proteins such as collagen, as well as the necessity for potentially cytotoxic chemical cross-linking to render these materials water stable, remains a detractor.[6]

Vitrification is a process that involves the gradual drying of a liquid medium resulting in a glass-like material and has been applied to various biological materials, including collagen.[7] Vitrification of collagen I gels results in thin, fibrous, water stable membranes which can naturally resemble the thickness and fiber diameter of human Bruch's membrane.[7,8] To this end, vitrified collagen materials have recently gained attention in numerous tissue engineering pursuits, including those related to the lung,[9−11] cornea,[11,12] placenta,[13,14] and, pertinent to this study, the outer retina.[15−17] We adopt an established protocol for producing fibrous collagen membranes, which have been identified to have biochemical composition and physical dimensions similar to that of human Bruch's membrane and characterize this material for a range of properties (*e.g.*, structural, mechanical, and diffusion) critical to the function of Bruch's membrane. We study the utility of this basal lamina-like surface-functionalized fibrous collagen I membrane as an *in vitro* Bruch's membrane mimetic and demonstrate material property advantages over commonly utilized, commercially available, porous PET Transwell membranes. Furthermore, for the first time, we characterize the performance of immortalized RPE, pluripotent stem cell-derived RPE and vascular endothelial cells with a basal lamina-functionalized fibrous collagen membrane.

2. MATERIALS AND METHODS

2.1. Vitrified Collagen Membrane Fabrication. This fabrication protocol was adapted from the optimized works of Takezawa *et al.* (2004) and Calderón-Colón *et al.* (2012).[7,8] Using a class II biosafety hood and aseptic technique, on ice, 1 part of chilled 10X phosphate buffered saline (PBS, Thermo Fisher Scientific, 70011044) was added to 8 parts of bovine type I atelocollagen solution (3 mg/mL) in 0.01 N HCl (PureCol, Advanced BioMatrix, 5005). The pH of the pregel mixture was adjusted to pH 7−7.5 using 0.22 μm sterile filtered 0.1 M NaOH and monitored using pH paper. A final volume of sterile distilled water (Thermo Fisher Scientific, 15230162) was added for a total of 10 parts volume. The pregel mixture was briefly centrifuged (200*g*, 5 s) to remove any air bubbles from the solution, then placed in tissue culture polystyrene (TCPS) well plates or layered on top of polytetrafluoroethylene (PTFE) substrates with transparent polyvinyl chloride (PVC) ring frames, at a concentration of 0.789 mg/cm^2. Pregel solutions were then incubated at 37 °C in an atmosphere of 5% (v/v) CO_2 in air for at least 2 h to facilitate gelation. Gels were then placed inside a class II biosafety hood (with lids off) to dry for 7 days. To remove residual salts, membranes were washed in triplicate with sterile distilled water and then redried overnight. Membranes were either used *in situ* or carefully peeled and lifted from PTFE substrates by the PVC frame using fine tip forceps (Figure S1). Membrane thickness was determined using a Dayton DDM025 digital micrometer (Sydney Tools, W137691).

2.2. Scanning Electron Microscopy. Vitrified collagen membranes were imaged *via* scanning electron microscopy (SEM) after the redrying step in Section 2.1. Samples were mounted on an aluminum stub with double-sided conductive carbon tape then iridium-coated using a Cressington 208HRD sputter coater. The thickness of the iridium coating was approximately 4 nm (60 mA for 30 s). Conductive coating is necessary to prevent charge accumulation in an electron microscope to obtain clear images, especially for an insulating material. The samples were imaged using a Zeiss Merlin FESEM (field emission SEM) operated in secondary electron mode to highlight topographical features. An accelerating voltage of 3−5 kV was used for imaging. The magnifications used are indicative of the scale bars in all of the images shown.

Fiber diameter distributions were derived from SEM images using ImageJ software. A minimum of 100 measurements were created using the imaging software to plot fiber diameter distributions, and results were reported as the mean ± standard deviation.

2.3. Mechanical Testing. *2.3.1. Uniaxial Tensile Testing.* Uniaxial tensile testing was performed using an Instron 5500R Frame equipped with a 100 N load cell and Bluehill3 software (version 3.04). Vitrified collagen membranes were prepared in large sheets, and dog-bone-shaped testing samples with a gauge length of 12.8 mm and width of 4.2 mm were punched out using an overhead mechanical lever punch. Samples were secured in pneumatic clamps layered with fine sandpaper to mitigate sample slippage. Only samples that displayed no indication of slippage and failed toward the middle of the gauge area were included for analyses.

2.3.2. Uniaxial Puncture Testing. Uniaxial puncture testing was performed using an Instron 5500R Frame equipped with a 100 N load cell and Bluehill3 software (version 3.04). Vitrified collagen membranes were prepared as 20 mm diameter disks, secured at the periphery using custom-made interlocking PTFE rings with an exposed 13 mm orifice, and finally mounted flat into a custom-built testing rig, perpendicular to the probe path (Figure S2A). Transwell PET membranes 0.4 μm pore size (Sigma-Aldrich, CLS3450) were removed from cell culture inserts and similarly secured using custom-made interlocking PTFE rings. A probe of 5 mm diameter and rounded tip of 2.5 mm radius was displaced at a rate of 10 mm/min from beneath and moved through the mounted sample until failure (Figure S2B). Only samples that ruptured from the middle of the sample outward (not those that ruptured around the perimeter of the sample) were included for analyses.

The maximum value of membrane stress was calculated like Bacakova *et al.*[18] as follows

$$\sigma(u_z \le a) = \frac{F_z}{2\pi R d \tan^{-1}\left(\frac{R}{u_z}\right)}$$

for the geometrical contact ratio, a: $a = \frac{f}{r}R$

where the membrane stress (σ) is a function of the sample radius (R), the probe radius (r), the membrane thickness (d) and the probe displacement (u_z).[18] A labeled diagram of these variables can be found at Bacakova *et al.*[18] Results were compared *via* a 2way ANOVA followed by a Šídák's multiple comparisons test using GraphPad Prism version 9.3.1.

2.4. Sessile Drop Test. Vitrified collagen membrane samples were taped down onto glass microscope slides to ensure that samples remained flat during testing. Samples were placed on the instrument

https://doi.org/10.1021/acsbiomaterials.4c01112
ACS Biomater. Sci. Eng. 2024, 10, 5653−5665

(SEO Contact Angle Analyzer model Phoenix MT-mat, with SEO Surfaceware V9.9 software) stage directly under the syringe needle. When the deionized water drop was initiated on the needle tip, samples were raised to touch the sample drop and then lowered below the needle tip, whereby recording was immediately initiated. The liquid-substrate interface was defined manually by the user in the software, and the contact angle was calculated automatically. Recording was conducted at room temperature and humidity. Initial and final contact angle values were compared *via* an unpaired t-test using GraphPad Prism version 9.3.1.

2.5. Membrane Diffusion Test. Vitrified collagen membranes treated with 10 mU/mL transglutaminase for 2 h at 37 °C and 5% CO_2, prepared as 20 mm diameter disks, and 0.4 μm pore size Transwell membranes were secured using custom-made interlocking PTFE rings, with an exposed 8.5 mm orifice, and secured between two glass cells, each with a 10 mL volume. Membranes were equilibrated three times with Dulbecco's PBS (DPBS, Thermo Fisher Scientific, 14190144) by 10 min immersion. Samples of either FITC-albumin (Sigma-Aldrich, A9771), FITC-dextran 20 kDa (Sigma-Aldrich, FD20S) or FITC-dextran 40 kDa (Sigma-Aldrich, FD40) were prepared in DPBS at 1 mg/mL and 10 mL placed in one cell. The remaining cell was filled with 10 mL DPBS. A 100 μL sample was taken from each cell hourly for a period of 6 h and fluorescence intensity determined on a PHERAStar microplate reader (BMG Laftech). A standard curve from 0.1 μg/mL to 2 mg/mL in the linear regime was determined and used to correlate emission intensity with unknown molecular concentration. All experiments were performed in triplicate and results reported as mean ± standard deviation. The permeability coefficient was calculated from the following equation derived from Fick's law[19]

$$\ln\left(1 - \frac{2C_t}{C_0}\right) = \frac{-2AU}{VL}t$$

where C_t is the concentration in the receiver cell at time t, C_0 is the initial concentration in the donor cell, A is the effective membrane area, L is the membrane thickness, V is the compartment volume, and U is the permeability coefficient. Results were compared *via* a 2way ANOVA followed by a Šídák's multiple comparisons test using GraphPad Prism version 9.3.1.

2.6. Biocompatibility Cell Culture Studies. Human cell lines utilized for this study were approved by the CSIRO Health & Medical Research Ethics Committee, approval 2020_066_LR.

2.6.1. Routine ARPE-19 and HUVEC Cell Culture. The spontaneously immortalized human retinal pigment epithelial cell line (ARPE-19, ATCC, CRL-2302), was routinely maintained in Dulbecco's modified Eagle medium-12 (DMEM-F12, Thermo Fisher Scientific, 11330032) supplemented with 10% (v/v) fetal bovine serum (FBS, Thermo Fisher Scientific, 10099141) on uncoated TCPS cultureware. Briefly, cultures were subcultured at an estimated confluence of 80−100% *via* 10 min/37 °C dissociation with 0.05% (w/v) Trypsin-EDTA solution (Thermo Fisher Scientific, 25300054) and replated at a ratio of 1:3 to 1:5, with complete media renewal every 2−3 days. To facilitate maturation in long-term cultures, ARPE-19 cells were cultured in DMEM-F12 with 1% (v/v) FBS, with complete media changes twice weekly.[20]

Human umbilical vein endothelial cells (HUVECs, StemCell Technologies, #HUVEC-001F-M) were routinely maintained on gelatin-coated cultureware in EBM-2 media (Lonza, CC-3156) supplemented with EGM-2 BulletKit (Lonza, CC-4176). TCPS cultureware was precoated with 0.5% (w/v) type B gelatin solution (Sigma-Aldrich, G1393) for 2 h at 37 °C, 5% CO_2 in air. Briefly, cultures were subcultured at an estimated confluence of 70−80% *via* 3−5 min/37 °C exposure to 0.25% (w/v) trypsin-EDTA (Thermo Fisher Scientific, 25200056) and replated at a density of 5000 cells/cm^2, with complete media renewal every 2 days. Control experiments conducted on TCPS, and tissue culture glass (TC glass), were conducted according to these protocols.

2.6.2. Membrane Preparation and Cell Seeding. Vitrified collagen membranes were prepared in TCPS well plates, as described in Section 2.1, and placed under the UV germicidal lamp of a class II biosafety hood for 1 h. Membranes were then immersed in a 2X solution (20 units/mL penicillin, 20 μg/mL streptomycin, and 0.50 μg/mL Amphotericin B), prepared from 100X stock solution of antibiotic-antimycotic (Thermo Fisher Scientific, 15240096), in DPBS for 1 h at room temperature, then washed with sterile distilled water with 1X antibiotic-antimycotic (10 units/mL penicillin, 10 μg/mL streptomycin, and 0.25 μg/mL Amphotericin B) for 3 × 10 min on an orbital shaker at 100 rpm to remove any residual salt from the vitrification process. Prepared membranes were either used immediately in culture or stored at 4 °C for a maximum of 1 week for future use.

A 20 mU/mL transglutaminase solution (Sigma-Aldrich, T5398) was prepared in DMEM (without glutamine, Thermo Fisher Scientific, 11960044) with 1X antibiotic-antimycotic and sterile filtered using a 0.22 μm syringe filter. Laminin-entactin-collagen IV solution (Merck-Millipore, 08-110) was diluted to 110 μg/mL in DMEM (without glutamine) with 1X of antibiotic-antimycotic. Equal volumes of transglutaminase and laminin-entactin-collagen solutions were mixed immediately before adding to membranes and then placed at 37 °C, 5% CO_2 in air for 1 h. Coating solutions were then aspirated and washed once more with sterile distilled water with 1X antibiotic-antimycotic, and cells were seeded on top of membranes or control substrates in their respective cell culture media. ARPE-19 cells were seeded at a density of 10,000 cells/cm^2 and HUVECs at 5000 cells/cm^2 (equivalent to subcultivation ratios recommended by suppliers).

For immunostaining of protein coatings, surface functionalized membranes were incubated in solutions of anti-laminin primary antibody (Sigma-Aldrich, L9393) for 2 h at room temperature, washed three times, 5 min each, with DPBS and incubated with anti-rabbit IgG H & L Alexa Fluor 488 (Table S1) for 1 h at room temperature, followed by another three 5 min washes in DPBS. Imaging was conducted using a Nikon ECLIPSE Ti inverted microscope with NIS-Elements software.

2.6.3. Live−Dead Staining. Stock solutions of Ethidium homodimer-1 and Calcein AM (Thermo Fisher Scientific, L3224) were diluted to 2 and 4 μM, respectively, in DPBS and briefly vortex-mixed to ensure homogeneity. Media was aspirated and cultures washed once with DPBS to remove any unbound cells. The staining solution was then placed on cultures and incubated at room temperature for 45 min. Green and red fluorescence images (as well as bright-field) were captured across four regions of interest per culture well. Total live and dead cell number counts were approximated by using ImageJ software.

2.6.4. PrestoBlue Viability. PrestoBlue cell viability reagent (Thermo Fisher Scientific, A13261) was diluted 1:10 (v/v) in fresh complete culture medium. Spent culture medium was aspirated from wells, replaced with PrestoBlue working solution, and incubated for 45 min at 37 °C, 5% CO_2 in air. Samples of 100 μL per well were then taken and prepared in Nunc F96 MicroWell Black Polystyrene Plates (Thermo Fisher Scientific, 237105). Fluorescence intensity was determined at an excitation wavelength of 560 nm and emission wavelength of 590 nm using a PHERAStar microplate reader (BMG Laftech). Results were compared *via* a 2way ANOVA followed by a Šídák's multiple comparisons test using GraphPad Prism version 9.3.1.

2.6.5. Immunofluorescent Staining and Imaging. For immunostaining assays, both membrane and control cultures were conducted in 8-well glass chamber slides (Thermo Fisher Scientific, 15434PK). Cultures were fixed at room temperature with 3.7% (w/v) paraformaldehyde (Electron Microscopy Sciences, 15710) for 10 min then washed with DPBS three times for 5 min each. Fixed cultures were then permeabilized with a 0.1% (w/v) Triton X-100 solution in DPBS for 10 min followed by three 5 min washes with DPBS, then incubated in 10% (v/v) normal goat serum (NGS, Thermo Fisher Scientific, 50062Z) blocking solution at 4 °C overnight. Cultures were then incubated in anti-ZO-1 IgG_1 (Thermo Fisher Scientific, 33-9100), anti-CD144 IgG_1 (VE-cadherin, Thermo Fisher Scientific, 14-1449-82) and IgG_1 isotype control (Thermo Fisher Scientific, 14-4714-82) primary antibodies, diluted as per Table S1 in 10% (v/v) NGS for 1 h at room temperature, followed by three

https://doi.org/10.1021/acsbiomaterials.4c01112
ACS Biomater. Sci. Eng. 2024, 10, 5653−5665

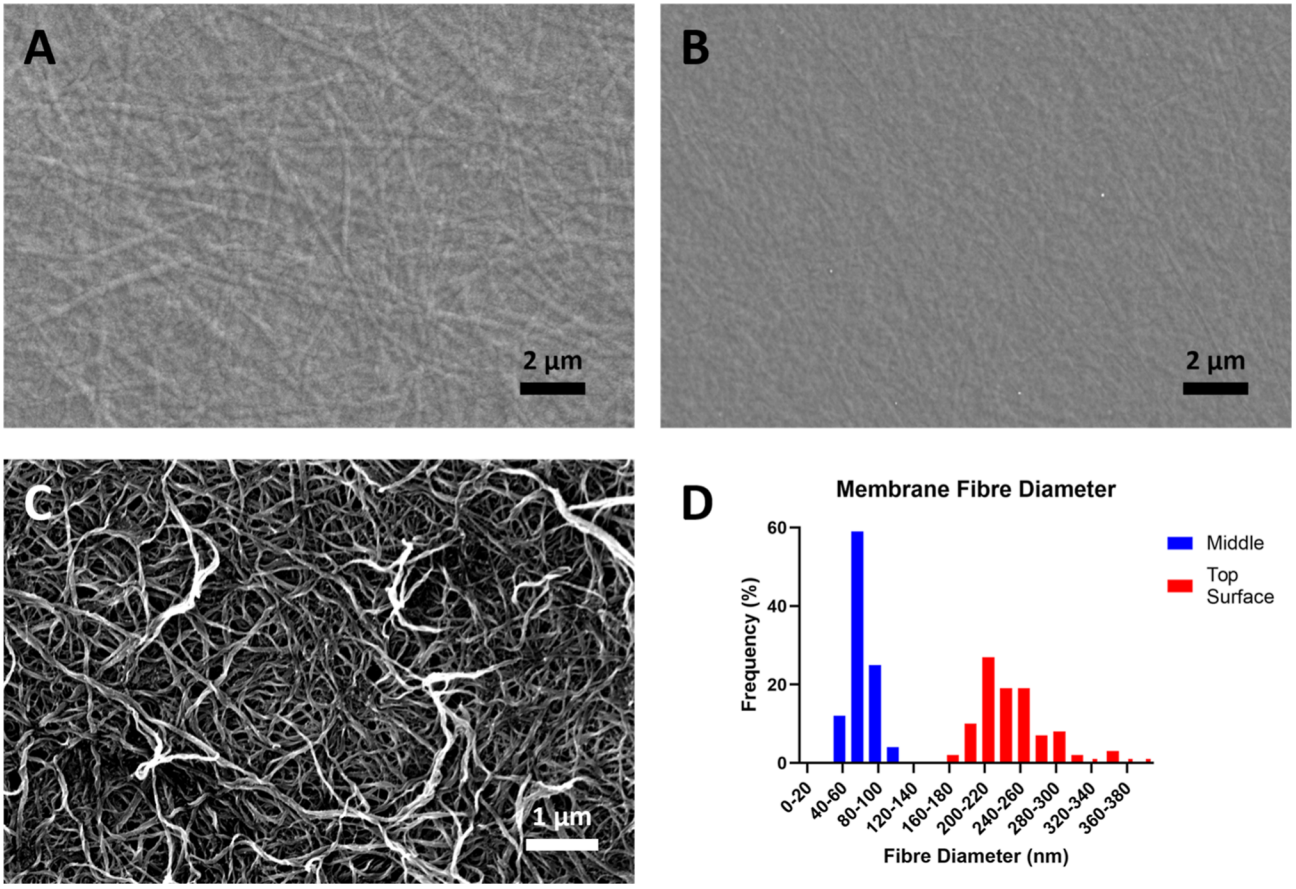

Figure 1. Vitrified collagen I membranes. SEM images of the membrane top [(A) scale bar = 2 μm], bottom [(B) scale bar = 2 μm] and middle [(C) scale bar = 1 μm] surfaces. (D) Fiber diameter frequency distributions of fibers present on the top surface and middle interior of the membrane. A lack of surface features in figures (A,B) results in reduced contrast when compared to figure (C).

5 min washes with DPBS. Secondary antibody anti-IgG1 AlexaFluor 488 (Thermo Fisher Scientific, A21121), diluted to 4 μg/mL in 10% (v/v) NGS, or Actin Green solution (Thermo Fisher Scientific, R37110) diluted 2 drops/mL in DPBS, was incubated for 1 h at room temperature, followed by another three 5 min washes with DPBS. 4′,6-Diamidino-2-phenylindole, dihydrochloride (DAPI) 5 mg/mL stock solution (Thermo Fisher Scientific, D1306) was diluted to 300 mM in DPBS, applied to cultures and incubated to 10 min at room temperature, followed by another three 5 min washes with DPBS. Finally, chamber gaskets were carefully removed, and replaced with rectangular coverslips, sealed with hard set mounting media (Thermo Fisher Scientific, P36934) and allowed to harden overnight. Samples were imaged using a Nikon ECLIPSE Ti inverted microscope with NIS-Elements software.

2.7. Human Stem Cell-RPE Differentiation Culture. *2.7.1. hESC Maintenance Culture.* WA09 (H9, WiCell Provider Dr. James Thomson, University of Wisconsin) human embryonic stem cell (hESC) cultures were maintained on Vitronectin XF-coated (StemCell Technologies, 071919) sterile non tissue culture-treated polystyrene 6-well plates (StemCell Technologies, 27147) and maintained in complete TeSR-E8 medium (StemCell Technologies, 05990). Briefly, 6-well plates were coated in 10 μg/mL Vitronectin XF solution diluted in CellAdhere dilution buffer (StemCell Technologies, 071919) for 1 h at room temperature. HESC cultures were passaged in aggregate form after washing with DPBS (no calcium, no magnesium) and exposure to ReLeSR cell dissociation reagent (StemCell Technologies, 071919) for 1 min and a further 7−9 min after ReLeSR aspiration. Cell aggregates were harvested *via* the addition of TeSR-E8 medium and gentle tapping of the plate for 1 min to release cell aggregates. Cell aggregate mixtures were replated on Vitronectin XF coated plates at a dilution ratio of 1:8, with subsequent daily complete media renewal.

2.7.2. RPE Differentiation. HESCs were differentiated as previously described.[21] Briefly, hESCs were cultured until reaching confluency of 70−80%, at which stage TeSR-E8 medium was fully replaced with Complete E6 medium (StemCell Technologies, 05946) supplemented with 1X N-2 supplement (Thermo Fisher Scientific, 17502048) to induce retinal differentiation with three weekly complete medium exchanges for approximately 30 days. On day 33, retinal differentiation medium was completely replaced with RPE medium, consisting of α-MEM (Thermo Fisher Scientific, 12571063) supplemented with 5% (v/v) FBS (Thermo Fisher Scientific, 10099141), 1X nonessential amino acids (Thermo Fisher Scientific, 11140050), 100 U/mL penicillin−streptomycin (Thermo Fisher Scientific, 15140122), 1X N1 (Sigma-Aldrich, N6530), 0.25 mg/mL taurine (Sigma-Aldrich, T8691), 0.013 ng/mL 3,3′,5-triiodo-L-thytonine sodium salt (Sigma-Aldrich, T5516), 0.02 μg/mL hydrocortisone (Sigma-Aldrich, H6909), and 1X GlutaMAX (Thermo Fisher Scientific, 35050061) to promote RPE maturation. Media was replenished every second day for up to a further 50 days until maximum pigmentation was achieved by microscopic assessment.

RPE-like cells were harvested from differentiation cultures *via* an 8 min exposure to 0.25% (w/v) trypsin-EDTA. Cells were counted and replated at a density of 75,000 cells/cm^2 onto functionalized vitrified collagen membranes (prepared as per Section 2.6.2) or growth factor-reduced Matrigel-coated (In Vitro Technologies, 354230) standard TCPS well plates and cultured for a further 28 days. Cultures were then fixed, permeabilized, blocked, immunostained, and mounted as per Section 2.6.5 using the primary antibodies anti-ZO-1 IgG$_1$, anti-CRALBP IgG$_1$ (Thermo Fisher Scientific, MA1-813), anti-MITF IgG$_1$

https://doi.org/10.1021/acsbiomaterials.4c01112
ACS Biomater. Sci. Eng. 2024, 10, 5653−5665

kappa (Thermo Fisher Scientific, Abcam, ab3201) and IgG_1 isotype control as per Table S1.

3. RESULTS

3.1. Membrane Morphology. Bovine collagen I membranes produced by the vitrification process, washed to remove any residual salts, and air-dried resulted in an average thickness of 7.33 ± 1.70 μm. The top (exposed to air during vitrification) and bottom (in contact with PTFE substrate) surface of the material were visualized by SEM to reveal a semiamorphous fibrous morphology (Figure 1A) and an amorphous flat morphology, respectively (Figure 1B). Small regions of the membrane that had undergone delamination during the substrate detachment process revealed a distinctive fibrous morphology within the membrane interior, termed the "middle" surface (Figure 1C). Membrane cross sections produced by tearing were observed to display a layered porous structure (Figure S3). Fiber thickness on the membrane top surface was measured to be 160−400 nm with an average of 221 ± 41.9 nm, and fiber thickness in the membrane middle measured to be 40−120 nm with an average of 53.0 ± 12.9 nm (Figure 1D). No discernible fibers were detected on the membrane bottom surface.

3.2. Mechanical Testing. Dry vitrified collagen membranes, extended to break under uniaxial strain at a rate of 10 mm/min, displayed *j*-shaped stress−strain curves with an average tensile strength of 17.7 ± 2.51 MPa, strain at break of 0.04 ± 0.01 mm/mm, and elastic modulus of 638 ± 88.6 MPa (Figure S4 and Table S2).

Both dry and hydrated forms of vitrified collagen membranes were also evaluated for mechanical performance subject to a membrane puncture test and displayed similar *j*-shaped force−extension curves (Figure S5) to those of the uniaxial tensile test (Figure S4). Vitrified collagen membranes of mean thickness 10 ± 2.0 μm displayed a rupture force of 17.0 ± 0.58 N, maximum extension of 4.04 ± 0.16 mm, and rupture stress of 42.8 ± 9.61 MPa when dry; and a rupture force of 0.15 ± 0.03 N, maximum extension of 5.02 ± 0.42 mm, and rupture stress of 0.39 ± 0.07 MPa when hydrated (Table 1). PET control membranes of mean thickness 12.0 ± 0.00 μm displayed a rupture force of 20.0 ± 1.30 N, maximum extension of 3.38 ± 0.10 mm, and rupture stress of 37.4 ± 2.84 MPa when dry; and a rupture force of 21.1 ± 0.58 N, maximum extension of 3.70 ± 0.06 mm, and rupture stress of 41.0 ± 1.36 MPa when hydrated (Table 1). When hydrated, vitrified collagen membranes displayed a statistically significant reduction in both rupture force ($P < 0.001$) and rupture stress ($P < 0.001$) compared to those in the dry state. There was no significant difference in the rupture stress for the PET membrane when hydrated.

Table 1. Membrane Puncture Testing Results[a]

	rupture force (N)	maximum extension (mm)	rupture stress (MPa)
collagen (dry)	17.0 ± 0.58	4.04 ± 0.16	42.8 ± 9.61
collagen (hydrated)	0.15 ± 0.03	5.02 ± 0.42	0.39 ± 0.07
PET (dry)	20.0 ± 1.30	3.38 ± 0.10	37.4 ± 2.84
PET (hydrated)	21.1 ± 0.58	3.70 ± 0.06	41.0 ± 1.36

[a]Rupture force (N), maximum extension (mm), and rupture stress (MPa) of vitrified collagen and porous PET membranes both dry and hydrated. Data were calculated from force−extension curves produced at a rate of 10 mm/min (n = 3, mean ± standard deviation).

3.3. Sessile Drop Test. Both dry vitrified collagen and PET membranes were subject to a deionized water sessile drop test to determine interfacial contact angle to infer membrane surface hydrophilicity and absorption capacity (Figures 2 and S6). Dry vitrified collagen membranes displayed an initial contact angle of 86.1 ± 4.47° and after 78 s, a final contact angle of 71.6 ± 3.73°, a statistically significant reduction of 16.8% ($P < 0.05$). Dry PET membranes displayed an initial contact angle of 60.7 ± 7.08° and after 78 s, a final contact angle of 49.1 ± 5.76°, a statistically significant reduction of 19.1% ($P < 0.05$). To account for any possible evaporation loss, the test was repeated on solid PTFE substrates and demonstrated a percentage reduction in contact angle of 1.59%.

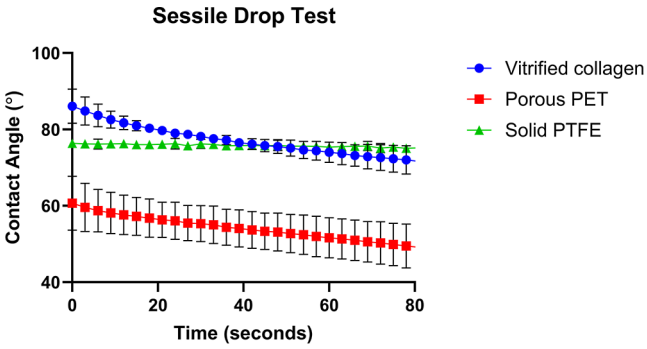

Figure 2. Membrane sessile drop test. The droplet contact angle of denoised water placed atop vitrified collagen and porous PET membranes was analyzed over a period of 78 s. A solid PTFE substrate was also analyzed to determine the influence of evaporation on the analyses. (N = 3, average ± standard deviation). PET = polyethylene terephthalate, PTFE = poly tetrafluoroethylene.

3.4. Membrane Permeability. The concentration of fluorescently tagged albumin, 20 kDa dextran, and 40 kDa dextran, across both transglutaminase-treated vitrified collagen and PET membranes, was quantified over a period of 6 h to determine the membranes' permeability coefficients Figure 3. The mean average permeability coefficient of the vitrified collagen membrane was found to be greater than that of the

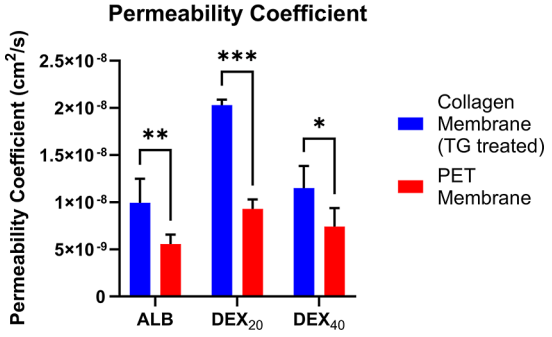

Figure 3. Membrane permeability coefficients. The permeability coefficients of both TG-treated vitrified collagen and porous PET membranes were determined using fluorescently labeled albumin, dextran 20 kDa and dextran 40 kDa. (N = 3, mean ± standard deviation). ALB = FITC-albumin, DEX_{20} = FITC-dextran 20 kDa, DEX_{40} = FITC-dextran 40 kDa, FITC = fluorescein isothiocyanate and TG = transglutaminase.

https://doi.org/10.1021/acsbiomaterials.4c01112
ACS Biomater. Sci. Eng. 2024, 10, 5653−5665

PET membrane for all molecules with the difference being statistically significant for FITC-albumin ($P < 0.05$), FITC-dextran 20 kDa ($P < 0.001$), and FITC-dextran 40 kDa ($P < 0.05$).

3.5. Surface Functionalization. Vitrified collagen membranes were surface functionalized with a laminin, collagen IV, and entactin protein mixture by physical adsorption and enzymatic cross-linking. The presence of laminin on the membrane surface was observed *via* both attachment methods by immunofluorescent staining (Figure 4). The intensity of

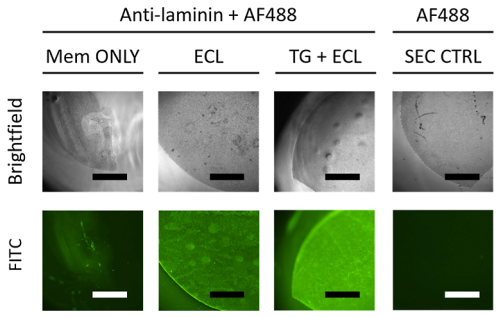

Figure 4. Surface functionalization of vitrified collagen membranes. Vitrified collagen membranes without coating (Mem), with physically adsorbed ECL coating (ECL) and with enzymatically bound ECL coating with transglutaminase (TG + ECL) compared with secondary antibody only control (SEC CTRL) immunofluorescently stained for the laminin subunit α1. Images display the membrane in both the brightfield and FITC imaging channels (all scale bars = 1 mm). Mem = vitrified collagen membrane, ECL = entactin, collagen IV and laminin, TG = transglutaminase, SEC CTRL = secondary control, and AF488 = AlexFluor 488.

detected staining was observed to be higher on the enzymatically bound surface than on those physically adsorbed. Collagen membranes without coating displayed insignificant amounts of fluorescence.

3.6. ARPE-19 Biocompatibility. ARPE-19 cells were cultured on vitrified collagen membranes with, no functionalization, transglutaminase enzyme, physically adsorbed laminin-collagen IV-entactin, enzymatically bound laminin-collagen IV-entactin and control TCPS, to systematically determine the influence of the collagen membrane and all coating components on ARPE-19 cell health. After 6 days, all conditions demonstrated cell viability *via* live/dead staining over 98.9%, with no statistically significant variance between any of the conditions (Figures 5A and S8A). Using the same conditions, total culture metabolic activity was assessed between day 3 to day 7 of culture using the Presto Blue resazurin molecule, with results displaying a statistically significant increase in activity over the 4 day period ($P < 0.05$) for all conditions, and no statistically significant variation between each of the conditions (Figure 5B). After 80 days culture on enzymatically functionalized vitrified collagen membranes and tissue culture glass (control), ARPE-19 cultures were immunostained for fluorescent detection of the protein ZO-1, which was observed to be most pronounced at the cell−cell junctions on both materials [Figure 5C(ii,v)]. F-actin staining of cultures was also positive and pronounced at cell−cell junctions [Figure 5C(iii,vi)], and bright-field images revealed a cobblestone-like morphology on both materials [Figure 5C(i,iv)].

3.7. HUVEC Biocompatibility. HUVECs cultured on functionalized vitrified collagen membranes and control TCPS for 6 days demonstrated cell viabilities *via* live/dead staining of 96.8 and 97.4%, respectively, with no statistically significant difference between the two conditions (Figure 6A). Total culture metabolic activity was assessed from day 3 to day 7 using the resazurin molecule, with results showing a statistically significant increase in activity over the 4 day period for both conditions ($P < 0.05$) and no statistically significant difference between the two substrates (Figure 6B). After 7 days of culture on enzymatically functionalized vitrified collagen membranes and tissue culture glass (control), HUVEC cultures were immunostained for fluorescent detection of the proteins VE-cadherin [Figure 6C(i,iv)] and ZO-1 [Figure 6C(ii,v)], revealing a presence most pronounced at the cell−cell junctions on both materials. F-actin staining of cultures was also positive and pronounced at cell−cell junctions [Figure 6C(iii,vi)].

3.8. hESC-RPE Immunocytochemical Characterization. After at least 60 days of differentiation culture on vitronectin-coated untreated TCPS, distinct islands of pigmented cells were observed distributed throughout hESC-derived cultures (Figure S10). Upon replating these onto functionalized vitrified collagen membranes or Matrigel-coated TCPS control plates, both pigmented and nonpigmented cells were visually observed to have attached with high efficiency. As cultures continued to mature over a 28 day period, nonpigmented cells exited cultures, allowing pigmented cells to dominate. After 28 days of culture on functionalized vitrified collagen membranes and Matrigel-coated TCPS, cells developed a cobble stone-like morphology with most cells displaying visible pigmentation *via* color optical microscopy [Figure 7A(i),B(i)]. Immunofluorescent characterization of cells cultured on functionalized vitrified collagen membranes and Matrigel-coated TCPS controls demonstrated detected expression of the proteins ZO-1 [Figure 7A(ii),B(ii)], CRALBP [Figure 7A(iii),B(iii)] and MITF [Figure 7A(iv),B-(iv),B(iv)], as well as fluorescent staining for filamentous actin [Figure 7A(v),B(v)].

4. DISCUSSION

This study has demonstrated at concept scale the fabrication, by vitrification, of a functionalized collagen membrane, which supports long-term (up to 80 days with ARPE-19 and 28 days with hESC-RPE) human RPE cell cultures. This provides proof of concept for an outer retinal *in vitro* model akin to a human RPE-Bruch's membrane structure. These membrane materials can be produced entirely under aseptic conditions, without complex fabrication equipment, and are naturally water stable, without the requirement for potentially cytotoxic postprocessing. Additionally, these materials can mimic the naturally fibrous collagen morphology of human Bruch's membrane and, when functionalized with basement membrane proteins, can further represent the complex basal lamina. For comparison, SEM images of human Bruch's membrane can be found at the following ref 22. Holistically, these materials provide a more accurate physical representation of the human Bruch's membrane than synthetic alternatives and represent an approach toward a more physiologically accurate component for *in vitro* models of the outer retina.

Bovine collagen I membranes were produced by the vitrification process at a minimum thickness of 7.33 ± 1.70 μm, approximately 2−3 times thicker than human Bruch's

https://doi.org/10.1021/acsbiomaterials.4c01112
ACS Biomater. Sci. Eng. 2024, 10, 5653−5665

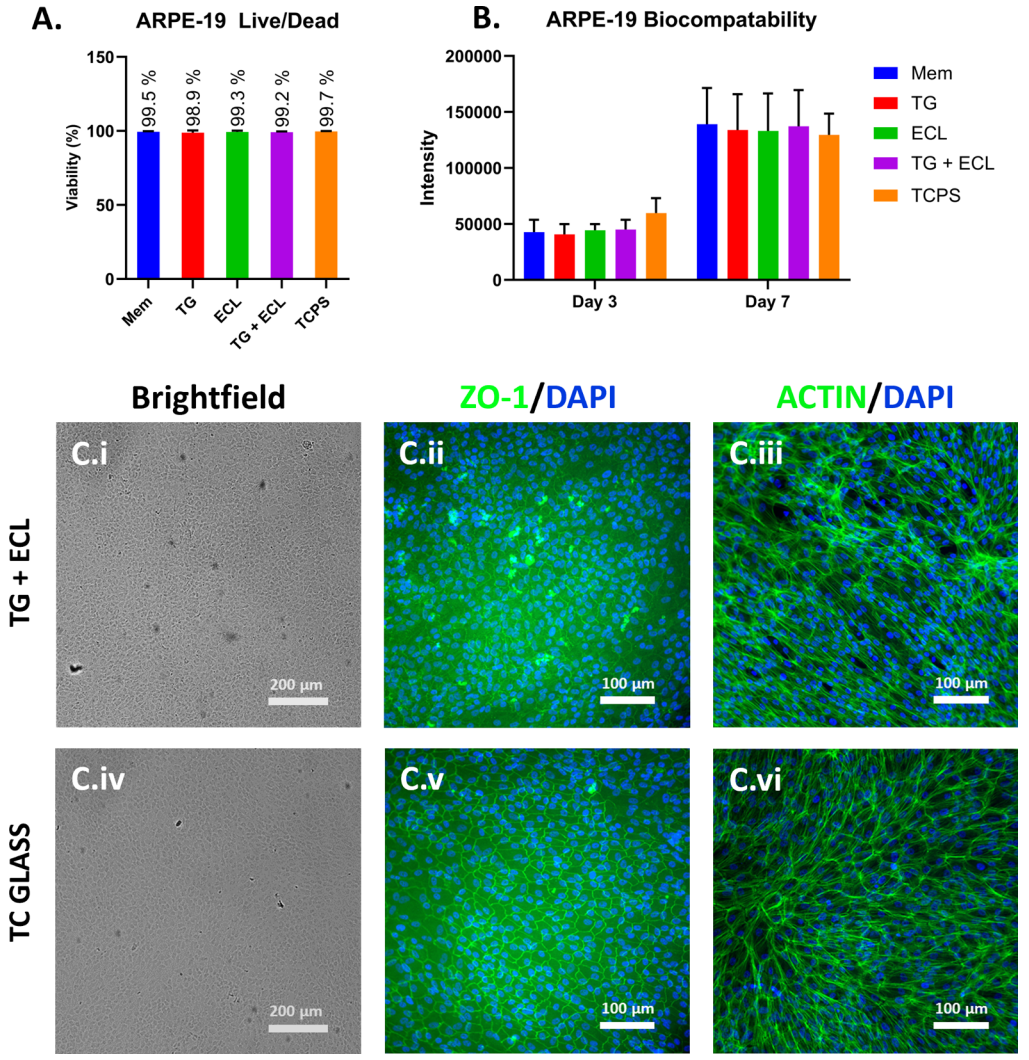

Figure 5. ARPE-19 cell biocompatibility and phenotypic analysis. (A) ARPE-19 cells cultured on vitrified collagen membranes with no coating (Mem), transglutaminase enzyme (TG), physically adsorbed entactin collagen IV laminin (ECL), enzymatically bound entactin collagen IV laminin (TG + ECL) and TCPS control. Quantitative results of live and dead cell counts are expressed as percentage live. (B) PrestoBlue culture viability of ARPE-19 cells at days 3 and 7 cultured on vitrified collagen membranes with no coating (Mem), transglutaminase enzyme (TG), physically adsorbed entactin collagen IV laminin (ECL), enzymatically bound entactin collagen IV laminin (TG + ECL) and TCPS control. (C) ARPE-19 cells cultured for 80 days on enzymatically functionalized membranes (i–iii) and control tissue culture glass (iv–vi). Representative brightfield images [(i,iv) scale bar = 200 μm], immunocytochemical staining for the tight junction protein ZO-1 [(ii,v) scale bar = 100 μm] and chemical staining for filamentous actin [(iii,vi) scale bar = 100 μm]. Representative isotype antibody and secondary antibody only control stains, Figure S8B. Mem = vitrified collagen membrane, TG = transglutaminase, ECL = entactin, collagen IV and laminin, TCPS = tissue culture polystyrene, TC = tissue culture and DAPI = 4′,6-diamidino-2-phenylindole.

membrane at 2.0–4.7 μm (aged 6–100 years old, determined *via* histological examination).[23,24] Micrometer-based measurements were used in this study to determine the membrane thickness. It should be noted that physical contact between the dry membrane and the micrometer measuring faces could introduce error into thickness measurements (proportional to excessive pressure applied) and propagate error to mechanical and diffusion testing. Contactless thickness measurements, such as noncontact profilometry, could be used to give greater accuracy in membrane thickness determination. Practically, producing membranes thinner than 7 μm was found to be difficult, as manually removing the membrane from the casting substrate resulted in tearing and membrane damage. Improved methods for fabricating thinner membranes without damage, such as the suspended approach developed by Newton *et al.*,[25] could potentially improve this material's ability to accurately model the molecular transport properties of the native membrane. The structures of the top, internal, and bottom surfaces of vitrified collagen membranes were all found to exhibit different morphology *via* SEM. The top surface of the membrane visually revealed a semiamorphous-like network of fibers, which likely resulted from a reduction in crystallinity during the 7 day, room temperature drying process. The diameter of these semiamorphous fibers was greater than that of the outer collagenous layer of the adult human Bruch's membrane, 40–100 nm.[22,23,26] The middle layer of the vitrified collagen membrane exhibited a more crystalline fibrous collagen-like structure, with a fiber diameter range of 40–120 nm, consistent with the fibers of the native adult human Bruch's membrane inner collagen layer, 40–100 nm.[22,23,26] The underside or bottom surface of the membrane, cast in direct contact with the PTFE substrate, displayed limited

https://doi.org/10.1021/acsbiomaterials.4c01112
ACS Biomater. Sci. Eng. 2024, 10, 5653–5665

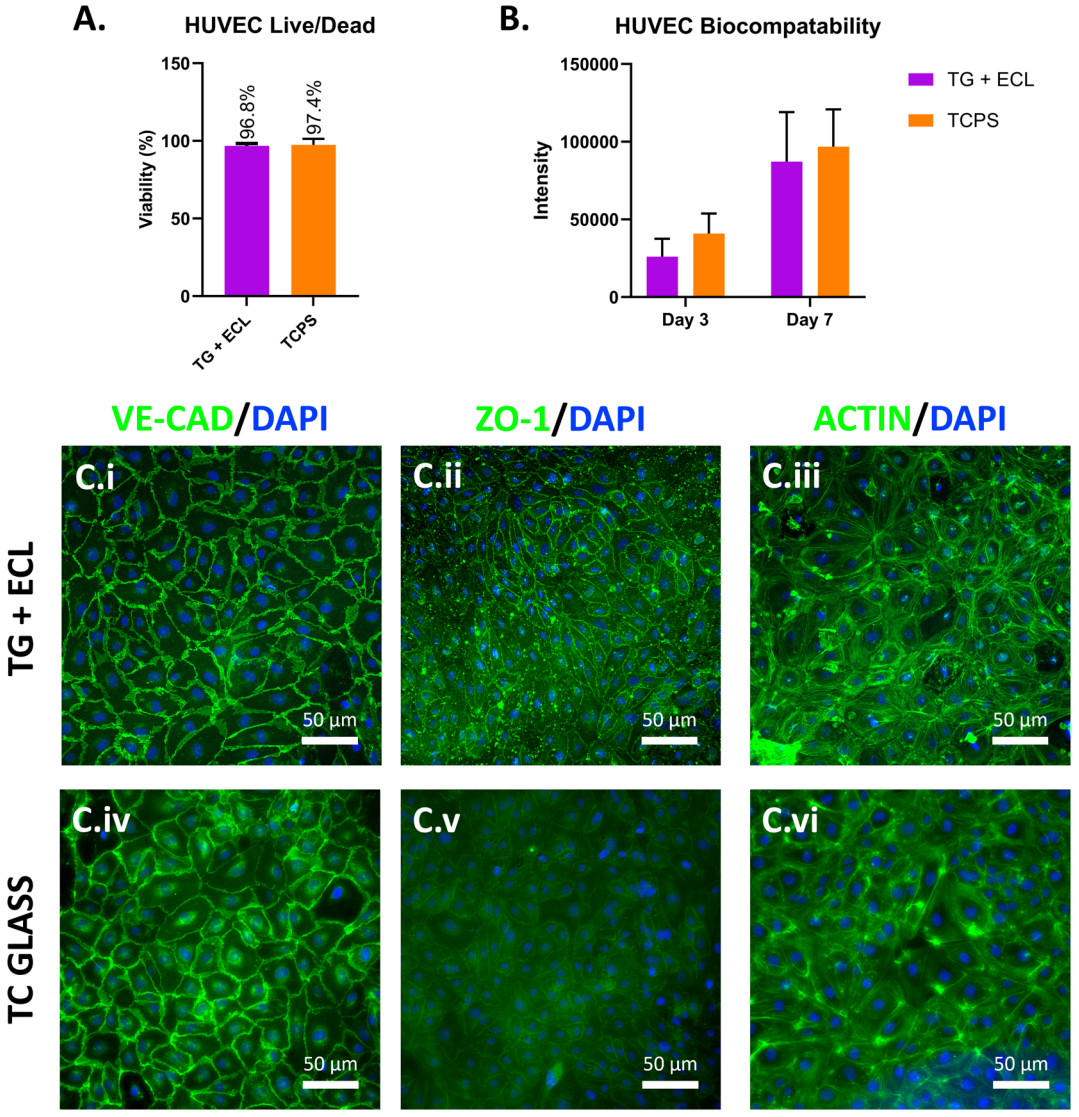

Figure 6. HUVEC biocompatibility and phenotypic analysis. (A) HUVECs cultured on vitrified collagen membranes with enzymatically bound entactin collagen IV laminin (TG + ECL) and TCPS control. Quantitative results of live and dead cell count expressed as percentage live. (B) PrestoBlue culture viability of HUVECs at day 3 and 7 cultured on vitrified collagen membranes with enzymatically bound entactin collagen IV laminin (TG + ECL) and TCPS control. (C) HUVECs culture for 7 days on enzymatically functionalized membranes (i–iii) and control tissue culture glass (iv–vi). Immunocytochemical staining for the tight junction proteins VE-cadherin (i,iv), ZO-1 [(ii,v) scale bar = 100 μm] and chemical staining for filamentous actin [(iii,vi) scale bar = 50 μm]. Representative isotype antibody and secondary antibody only control stains Figure S9B. Mem = vitrified collagen membrane, TG = transglutaminase, ECL = entactin, collagen IV and laminin, TCPS = tissue culture polystyrene, TC = tissue culture, and DAPI = 4′,6-diamidino-2-phenylindole.

evidence of fibrous morphology, likely resulting from the interface preventing stable fiber formation. Detachment of vitrified collagen membranes was found to be best when cast onto PVC circular frames and when the membrane was dried after salt removal washing. This allowed for easy handling without membrane damage, and the attachment of a substrate prevented major shrinking of membranes when redrying. Production of the vitrified collagen membrane takes up to 7 days and occurs in a sterile environment, which potentially could be modified or optimized for consideration to industrial translation.

Tensile testing of vitrified collagen membranes resulted in a *j*-shaped stress–strain curve, which is typical of most soft biological tissue, and the human retina, and is generally characteristic of collagen fiber elongation.[27] To our knowledge there are no studies evaluating the mechanical properties of the human Bruch's membrane (without attached choroid) *via* uniaxial tensile testing.[4] A study of porcine Bruch's membrane–choroid complex in a hydrated form reported an elastic modulus of 2.44 MPa at 5% strain,[28] however, this result cannot be directly correlated to that obtained here for the vitrified collagen membrane, as this material was tested in a hydrated form and modulus was determined in the toe region of the stress–strain curve.

To address the dimensional limitations of uniaxial tensile testing, a puncture test was chosen to better approximate the circumferential forces the eye (and Bruch's membrane) experiences during changes in intraocular pressure and mechanical deformation.[27] While there exists no direct mechanical characterization of human Bruch's membrane subject to a uniaxial puncture test, in this study, hydrated vitrified collagen membrane demonstrated force–extension

https://doi.org/10.1021/acsbiomaterials.4c01112
ACS Biomater. Sci. Eng. 2024, 10, 5653–5665

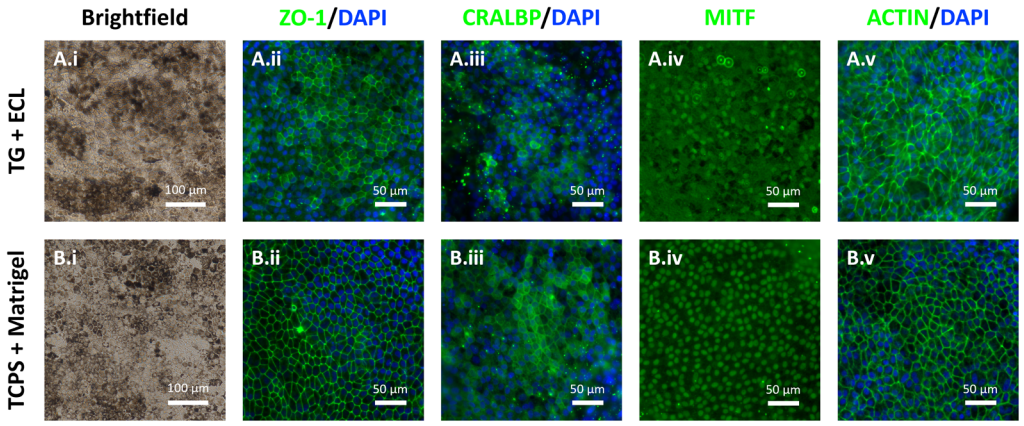

Figure 7. HESC-derived RPE-like cells on functionalized vitrified collagen membranes. HESC-derived RPE-like cells from >60 days differentiation culture was seeded to functionalized vitrified collagen membrane [TG + ECL, (A)] and Matrigel-coated TCPS control (B) for a further 28 days culture. Color brightfield images [(i) scale bars = 100 μm], immunocytochemical staining for the proteins ZO-1 (ii), CRALBP (iii), and MITF [(iv) scale bars = 50 μm], and chemical staining for filamentous actin [(v) scale bars = 50 μm]. IgG1 isotype control (Figure S11). Mem = vitrified collagen membrane, TG = transglutaminase, ECL = entactin, collagen IV and laminin, TCPS = tissue culture polystyrene, ZO-1 = zonula occludens-1, CRALBP = cellular retinaldehyde binding protein 1, MITF = melanocyte inducing transcription factor, and DAPI = 4′,6-diamidino-2-phenylindole.

profiles comparable to other biological membranes, such as that of the human fetal amnion.[29] Notably, hydrated vitrified collagen membranes exhibit a greater than 10-fold reduction in rupture stress when compared to the nonhydrated condition. This considerable softening was not evident with synthetic porous PET membranes, highlighting their limited ability to mimic the change in mechanical properties upon hydration, like that seen with most biological membranes. Both tensile and puncture testing was conducted on untreated vitrified collagen membranes. As transglutaminase (used in the surface functionalization strategy) is known to cross-link collagen molecules, it is expected that collagen membranes treated with transglutaminase would display increased mechanical properties for both tensile and puncture tests.

A sessile drop test and contact angle measurement was conducted to determine the surface hydrophilicity properties of vitrified collagen membranes compared to commercially available PET membranes and assess their ability to absorb and perfuse aqueous liquid. The contact angle of water on vitrified collagen membranes was found to be significantly greater and consequently less hydrophilic than that of the PET membrane. This is mostly likely influenced by the tissue culture plasma treatment process undertaken by the supplier to render the PET membranes with increased hydrophilicity,[30] a process not undertaken on the vitrified collagen membranes in this study. Both vitrified collagen and PET membranes displayed a significant reduction in water droplet contact angle during the 78 s study, indicating the ability of both materials to either absorb or perfuse the liquid into or through the membranes.

As well as altering membrane mechanical properties, transglutaminase is expected to potentially influence diffusion properties. For this reason, diffusion testing was conducted on TG-treated collagen membranes. The permeability coefficient of transglutaminase-treated vitrified collagen membranes was found to be roughly double that of PET membranes for fluorescently conjugated albumin, 20 kDa dextran, and 40 kDa dextran. The diffusion coefficient of 21.2 kDa FITC-dextran across adult human Bruch's membrane−choroid complex has been reported to be 6.80×10^{-7} cm^2/s,[31] compared to 2.03×10^{-8} cm^2/s for 20 kDa across vitrified collagen membranes. Optimisation of surface porosity on membrane exterior may further increase overall membrane permeability, as the amorphous and semiamorphous-like layers on the bottom and top surfaces of the vitrified collagen membrane, respectively, are suspected to limit the permeability coefficient. Nonetheless, transglutaminase-treated vitrified collagen membranes display permeability properties nearer to reported values for native human Bruch's membrane than commonly utilized commercially available PET membranes. Molecular weight cutoff is an important membrane characteristic which allows for selective transport of nutrients across Bruch's membrane. The molecular weight cutoff of human Bruch's membrane is age-dependent and has broadly been estimated to be 100−200 kDa.[32] To determine the selectivity of functionalized vitrified collagen membranes, molecular weight cut off should be evaluated in future studies.

Vitrified collagen membranes largely mimic the biomolecular composition of the inner and outer collagenous layers of the human Bruch's membrane; however, they do not possess surface ECM molecules to mimic that of the Bruch's membrane's basal lamina. Additionally, the long-term retention of *in vitro* RPE monolayers, particularly those derived from pluripotent stem cells, has been shown to be challenging on unfunctionalized novel membrane materials, such as silk fibroin.[33] To improve the physiological relevance of vitrified collagen membranes and potentially aid long-term retention of RPE monolayers, vitrified collagen membranes were enzymatically functionalized, using the enzyme transglutaminase, with a mixture of proteins; laminin, collagen IV and entactin. These proteins were selected as they are abundant in the Bruch's membrane-RPE basal lamina and play a pivotal role in RPE behavior.[34] Immunofluorescent detection of the protein laminin revealed its presence on the membrane surface after enzymatic coupling. Laminin is the major component of the ECL mixture; therefore, laminin was chosen as the molecule to validate surface functionalization. As both collagen IV and entactin possess similar glutamic acid residues, it is predicted that these molecules functionalize to the membrane surface in a similar fashion to laminin. Interestingly, the presence of laminin was also detected on the coating physically adsorbed

https://doi.org/10.1021/acsbiomaterials.4c01112
ACS Biomater. Sci. Eng. 2024, 10, 5653−5665

to the membrane surface, however, at a lesser intensity, possibly due to protein removal occurring during the washing procedure, highlighting the importance of the enzymatic coupling to chemically bind the ECM proteins to the membrane surface.

The spontaneously immortalised human retinal pigment epithelial cell line, ARPE-19, was utilized to assess the short-term biocompatibility of functionalized vitrified collagen membranes. The functionalized vitrified collagen membrane, or its individual coating components, demonstrated no significant variation in cell viability after 6 days of culture when compared to TCPS control substrates, indicating the transglutaminase enzyme nor the protein coating mixture had any detrimental effect on ARPE-19 cell viability. While ARPE-19 cells on collagen membranes began to slightly ball up post exposure to the live/dead staining solution [Figure S8A(ii)], this did not influence cell viability [Figure 5A(i)] and a cobble stone-like morphology was visible on both membrane and control conditions during live culture [Figure 5C(i,iv)]. ARPE-19 cultures were shown to have a significant increase in overall metabolic activity between days 3 and 7 of culture with no variation across all testing conditions, confirming the surface functionalization process to not have any detrimental effect on ARPE-19 cell viability and was determined appropriate to take forward into long-term culture and phenotypic analyses. ARPE-19 cultures were continued to a total of 80 days to encourage the formation of tight epithelial cell−cell junctions, characteristic of the native RPE. After 80 days culture in a minimal serum-containing maturation medium, ARPE-19 cells grown on both functionalized vitrified collagen membranes and tissue culture glass microscope slides demonstrated a cobble-stone-like morphology and positive staining for the junctional cell markers, ZO-1 and F-actin, localized most strongly at cell−cell interfaces, both characteristic of native RPE. Qualitatively the expression of ZO-1 in ARPE-19 monolayers appears to be somewhat more abundant when cultured on tissue culture glass; however, future studies should investigate a more quantitative means of assessment to fully determine if this is the case. It is hypothesized that the surface roughness of the vitrified collagen membranes could somewhat retard the formation of a flat, tightly packed cell monolayer, compared to those on smoother tissue culture glass. It should be noted that TCPS and glass are *control* substrates, which do not represent the physical and biochemical properties of Bruch's membrane, nor have potential for *in vivo* implantation application, unlike vitrified collagen membranes. To further probe the formation of appropriately tight junctions within these long-term cultures, the expression of the transmembrane protein Claudin-19, or its corresponding gene *CLDN19* should be investigated, alongside TEER measurements.[20] After the 80 day culture period, cell-membrane constructs could be easily lifted off tissue culture glass slides in a single continuous piece, demonstrating that the membrane material did not suffer any significant degradation over this period and is suitable for supporting long-term *in vitro* epithelial cell studies.

As well as the RPE, Bruch's membrane also interacts with choriocapillaris, a network of blood vessels responsible for transporting nutrients and waste to and from the retina, respectively. While a monolayer of endothelial cells does not represent the multicellular and anatomical complexity of a blood vessel network such as the choriocapillaris, this approach was employed as a technically simpler method to assess the biocompatibility of functionalized vitrified collagen membranes with vascular endothelial cells. Having first demonstrated no significant reduction in cell viability of ARPE-19 cells on all iterations of membrane surface functionalization, human umbilical cord-derived vascular endothelial cell cultures were evaluated only on enzymatically functionalized membranes and compared to standard tissue culture surface controls. Like the ARPE-19 observations, HUVECs demonstrated no significant reduction in culture viability over a 7 day period, indicating suitable biocompatibility with this human endothelial cell type. After 7 days culture, HUVECs were shown by immuno-fluorescent staining and imaging to express the vascular cell-specific junctional protein VE-cadherin at cell−cell interfaces on both functionalized vitrified membranes and tissue culture glass slides. Similarly, cultures on both substrates demonstrated the localization of the junctional protein ZO-1 and F-actin, also at cell−cell interfaces. These results indicate the suitability of vitrified collagen membranes to facilitate the attachment and proliferation of an endothelial cell culture with a typical endothelial cell phenotype. Future studies would benefit from assessing the ability of human endothelial-stromal cell cocultures to self-assemble into perfusable vessel networks, similar to those studied by Paek *et al.*,[35] atop of functionalized vitrified collagen membranes. Such a system could give valuable insight into AMD pathogenesis associated with the choriocapillaris, such as increased vessel leakiness and neovascularization, and the influence this has on Bruch's membrane and RPE function.

The ability of the ARPE-19 cell line to mimic important RPE cell phenotype and function, such as the production of pigmentation and the formation of appropriate epithelial resistance is limited.[36,37] Pluripotent stem cell-derived RPE cells have been shown to better mimic the phenotype and functional characteristics of the native RPE and also provide a self-renewing source of RPE cells for *in vitro* studies, compared with sourcing primary human RPE cells. RPE-like cells differentiated *in vitro* from hESCs cultured on functionalized vitrified collagen membranes for 28 days were visually observed to adopt a cobblestone-like morphology with visible brown pigmentation [Figure 7A(i)], phenotypical of native RPE cells. The presence and regional specificity of a RPE phenotypic marker panel was confirmed in both membrane and control conditions, however, marker localization appeared to consistently be more specific in the control condition. RPE cells in membrane and control cultures were observed by immunofluorescent staining and image detection to express the proteins ZO-1 and F-actin predominantly at cell−cell junctions, however, this was morphologically observed to be somewhat more predominant in control cultures on Matrigel coated TCPS (which do not resemble Bruch's membrane nor could be implanted to the retina). Like the long-term ARPE-19 membrane cultures, it is hypothesized that potentially the surface roughness of the vitrified collagen membrane could retard the maturation of RPE cell monolayer cell−cell junctions. A longer-term study (>4 weeks) could produce a more pronounced localization of ZO-1 and F-actin at cell−cell junctions in membrane cultures, as has been demonstrated on unfunctionalized fibrous collagen membranes (6 weeks) and more generally on Matrigel-coated TCPS (up to 1 year).[17,21] RPE-like cells on both membrane and control cultures exhibited expression of the cytosolic protein CRALBP and the nuclear protein MITF, both characteristic of RPE cells. Functionalized vitrified collagen membranes demonstrate the ability to support the culture of a pigmented monolayer of

https://doi.org/10.1021/acsbiomaterials.4c01112
ACS Biomater. Sci. Eng. 2024, 10, 5653−5665

RPE-like cells with characteristic cobblestone-like morphology and the expression of phenotypic RPE proteins. Further functional characterization, such as TEER measurements, polarized secretion of growth factors, formation of apical microvilli, ability to phagocytose photoreceptor outer segments and *in vivo* animal retinal implantation studies will be required to demonstrate the ability of this material to support the formation of a functional RPE. Future studies could also investigate and interrogate the performance of disease-like states including induced pluripotent stem cell-derived RPE cells or disease-like degraded membrane hallmarks for the studying retinal diseases with a physiologically relevant membrane.[38,39]

A complex but reproducible *in vitro* model system which incorporates structures best representing the native phenotype and function of the RPE; the biomolecular, physical, and mechanical properties of the Bruch's' membrane; and the cellular, anatomical, and transport properties of the choriocapillaris will be most ideal for studying diseases of the outer retina. The functionalized vitrified collagen membrane reported in this study mimics a range of properties associated with the native human Bruch's membrane better than commercially available and commonly utilized synthetic porous PET Transwell insert membranes. However, some materials properties such as diffusion coefficient and total membrane thickness still fall short of the native Bruch's membrane. Additionally, further functional validation of RPE monolayers is necessary to fully validate material-supported cell function. The approach described here for producing vitrified collagen membranes could require considerable optimization to transition to a scalable sterile manufacture process. Assembly of membranes can be achieved, with moderate difficulty, into CellCrown NX inserts (Sigma-Aldrich), resulting in appropriate membrane tension, peripheral sealing, and limited damage; however, maintaining sterility in long-term cultures after this delicate manual assembly process was found to be challenging. Sterilization of preassembled constructs could be achieved by ethylene oxide gas treatment. The functionalized vitrified collagen membrane in this study incorporates a range of animal-derived materials (*e.g.*, bovine collagen) which potentially contribute an unknown influence on RPE cell phenotype and function and could limit future translation to humans. Ideally, this material would incorporate fully defined human analogues of these components; however, an increase in material cost should be considered if this approach is adopted. Future studies utilizing this material should look to incorporate RPE-endothelial vessel membrane coculture into a single system, potentially using a suspended well insert, to investigate the influence of coculture on the system. Such a system should also look to incorporate the dynamic transport profiles of endogenous and exogenous cytokines and growth factors by engineering liquid perfusion into membrane cocultures. Vitrified collagen membranes could also potentially have *in vivo* applications in RPE-Bruch's membrane cell implantation for the cessation or restoration of vision loss resulting from AMD. Vitrified collagen could have handling difficulties when hydrated, however, its resemblance in physical properties to products like that of amniotic membranes could inspire similar solutions, such as the poly(methyl methacrylate) frame used to secure amniotic membrane for corneal repair by ProKera or a degradable version of the frame utilized in this study, Figure S1.

5. CONCLUSIONS

Functionalized vitrified collagen membranes better mimic the physical, mechanical, and biomolecular properties of human Bruch's membrane than commonly utilized and commercially available synthetic porous PET membranes. The preparation of functionalized vitrified collagen membranes is simple, does not require specific fabrication equipment, can be done in bulk, and the final product does not require any cytotoxic post processing to render it water stable. This material was shown to be biocompatible with both ARPE-19 and HUVEC cultures and was demonstrated to support the establishment of a phenotypic hESC-derived RPE-like cell monolayer.

■ ASSOCIATED CONTENT

Supporting Information

The Supporting Information is available free of charge at https://pubs.acs.org/doi/10.1021/acsbiomaterials.4c01112.

Photographic images of vitrified collagen membranes, annotated images of uniaxial puncture testing rig, primary antibody details, SEM images of vitrified collagen membranes, tensile testing results of vitrified collagen membranes, puncture testing stress-extension plots, contact angle images, membrane diffusion profiles, live dead staining of ARPE-19 and HUVECs, isotype control staining images, and microscopy images of RPE-like cell differentiation (PDF)

■ AUTHOR INFORMATION

Corresponding Author

Veronica Glattauer − *Manufacturing, Commonwealth Scientific and Industrial Research Organisation, Clayton 3168 VIC, Australia;* orcid.org/0000-0001-9139-9720; Email: Veronica.Glattauer@csiro.au

Authors

Ashley R. Murphy − *Manufacturing, Commonwealth Scientific and Industrial Research Organisation, Clayton 3168 VIC, Australia;* Present Address: Maastricht University, Maastricht 6229ET, The Netherlands

Xuen Jen Ng − *Manufacturing, Commonwealth Scientific and Industrial Research Organisation, Clayton 3168 VIC, Australia;* Present Address: The University of Bayreuth, 95447 Bayreuth, Germany.

Grace Lidgerwood − *Department of Anatomy and Physiology, the University of Melbourne, Parkville 3010 VIC, Australia*

Alice Pébay − *Department of Anatomy and Physiology, the University of Melbourne, Parkville 3010 VIC, Australia; Department of Surgery, Royal Melbourne Hospital, the University of Melbourne, Parkville 3050 VIC, Australia*

Yen B. Truong − *Manufacturing, Commonwealth Scientific and Industrial Research Organisation, Clayton 3168 VIC, Australia;* orcid.org/0000-0003-2210-2414

Carmel M. O'Brien − *Manufacturing, Commonwealth Scientific and Industrial Research Organisation, Clayton 3168 VIC, Australia; Australian Regenerative Medicine Institute, Monash University, Clayton 3168, Australia*

Complete contact information is available at: https://pubs.acs.org/10.1021/acsbiomaterials.4c01112

Author Contributions

The manuscript was written through contributions of all authors. All authors have given approval to the final version of the manuscript.

Funding

CSIRO Research+ Postdoctoral Fellowship, research grant 2019−2022. Alice Pébay is supported by a NHMRC Research Fellowship (1154389).

Notes

The authors declare no competing financial interest.

■ ACKNOWLEDGMENTS

The authors would like to acknowledge the technical assistance of Mark Hickey with both uniaxial tensile and puncture mechanical testing.

■ ABBREVIATIONS

ALB, albumin; AMD, age-related macular degeneration; ARPE-19, adult retinal pigment epithelial cells; CD144, cluster of differentiation 144; CRALBP, cellular retinaldehyde-binding protein; DAPI, 4′,6-diamidino-2-phenylindole, dihydrochloride; DEX20, dextran 20 kDa; DEX40, dextran 40 kDa; DMEM, Dulbecco's modified Eagle medium; DMEM-F12, Dulbecco's modified Eagle medium-12; DPBS, Dulbecco's phosphate buffered saline; ECL, entactin-collagen IV-laminin; EDTA, ethylenediaminetetraacetic acid; FBS, fetal bovine serum; FITC, fluorescein isothiocyanate; hESCs, human embryonic stem cells; HUVECs, human umbilical vein endothelial cells; MEM, minimum essential medium; Mem, membrane; MITF, microphthalmia-associated transcription factor; NGS, normal goat serum; PBS, phosphate buffered saline; PET, polyethylene terephthalate; PTFE, polytetrafluoroethylene; PVC, polyvinylchloride; ROI, region of interest; RPE, retinal pigment epithelium; SEM, scanning electron microscopy; TC, tissue culture; TCPS, tissue culture polystyrene; TEER, transepithelial electrical resistance; TG, transglutaminase; VE-Cadherin, vascular endothelial-cadherin; ZO-1, zonula occludens-1

■ REFERENCES

(1) Flaxman, S. R.; Bourne, R. R. A.; Resnikoff, S.; Ackland, P.; Braithwaite, T.; Cicinelli, M. V.; Das, A.; Jonas, J. B.; Keeffe, J.; Kempen, J. H.; Leasher, J.; Limburg, H.; Naidoo, K.; Pesudovs, K.; Silvester, A.; Stevens, G. A.; Tahhan, N.; Wong, T. Y.; Taylor, H. R.; Bourne, R.; Ackland, P.; Arditi, A.; Barkana, Y.; Bozkurt, B.; Braithwaite, T.; Bron, A.; Budenz, D.; Cai, F.; Casson, R.; Chakravarthy, U.; Choi, J.; Cicinelli, M. V.; Congdon, N.; Dana, R.; Dandona, R.; Dandona, L.; Das, A.; Dekaris, I.; Del Monte, M.; deva, J.; Dreer, L.; Ellwein, L.; Frazier, M.; Frick, K.; Friedman, D.; Furtado, J.; Gao, H.; Gazzard, G.; George, R.; Gichuhi, S.; Gonzalez, V.; Hammond, B.; Hartnett, M. E.; He, M.; Hejtmancik, J.; Hirai, F.; Huang, J.; Ingram, A.; Javitt, J.; Jonas, J.; Joslin, C.; Keeffe, J.; Kempen, J.; Khairallah, M.; Khanna, R.; Kim, J.; Lambrou, G.; Lansingh, V. C.; Lanzetta, P.; Leasher, J.; Lim, J.; Limburg, H.; Mansouri, K.; Mathew, A.; Morse, A.; Munoz, B.; Musch, D.; Naidoo, K.; Nangia, V.; Palaiou, M.; Parodi, M. B.; Pena, F. Y.; Pesudovs, K.; Peto, T.; Quigley, H.; Raju, M.; Ramulu, P.; Rankin, Z.; Resnikoff, S.; Reza, D.; Robin, A.; Rossetti, L.; Saaddine, J.; Sandar, M.; Serle, J.; Shen, T.; Shetty, R.; Sieving, P.; Silva, J. C.; Silvester, A.; Sitorus, R. S.; Stambolian, D.; Stevens, G.; Taylor, H.; Tejedor, J.; Tielsch, J.; Tsilimbaris, M.; van Meurs, J.; Varma, R.; Virgili, G.; Wang, Y. X.; Wang, N.-L.; West, S.; Wiedemann, P.; Wong, T.; Wormald, R.; Zheng, Y. Global causes of blindness and distance vision impairment 1990−2020: a systematic review and meta-analysis. *Lancet Global Health* **2017**, *5* (12), e1221−e1234.

(2) Cuenca, N.; Maneu, V.; Lax, P. Current and future therapeutic strategies for the treatment of retinal neurodegenerative diseases. *Neural Regener. Res.* **2022**, *17* (1), 103−104.

(3) Loewa, A.; Feng, J. J.; Hedtrich, S. Human disease models in drug development. *Nature Reviews Bioengineering* **2023**, *1*, 545−559.

(4) Murphy, A. R.; Truong, Y. B.; O'Brien, C. M.; Glattauer, V. Bio-inspired human in vitro outer retinal models: Bruch's membrane and its cellular interactions. *Acta Biomater.* **2020**, *104*, 1−16.

(5) Warnke, P. H.; Alamein, M.; Skabo, S.; Stephens, S.; Bourke, R.; Heiner, P.; Liu, Q. Primordium of an artificial Bruch's membrane made of nanofibers for engineering of retinal pigment epithelium cell monolayers. *Acta Biomater.* **2013**, *9* (12), 9414−9422.

(6) Zeugolis, D. I.; Khew, S. T.; Yew, E. S.; Ekaputra, A. K.; Tong, Y. W.; Yung, L. Y.; Hutmacher, D. W.; Sheppard, C.; Raghunath, M. Electro-spinning of pure collagen nano-fibres - just an expensive way to make gelatin? *Biomaterials* **2008**, *29* (15), 2293−2305.

(7) Takezawa, T.; Ozaki, K.; Nitani, A.; Takabayashi, C.; Shimo-Oka, T. Collagen vitrigel: a novel scaffold that can facilitate a three-dimensional culture for reconstructing organoids. *Cell Transplant.* **2004**, *13* (4), 463−474.

(8) Calderón-Colón, X.; Xia, Z.; Breidenich, J. L.; Mulreany, D. G.; Guo, Q.; Uy, O. M.; Tiffany, J. E.; Freund, D. E.; McCally, R. L.; Schein, O. D.; Elisseeff, J. H.; Trexler, M. M. Structure and properties of collagen vitrigel membranes for ocular repair and regeneration applications. *Biomaterials* **2012**, *33* (33), 8286−8295.

(9) Mejías, J. C.; Nelson, M. R.; Liseth, O.; Roy, K. A 96-well format microvascularized human lung-on-a-chip platform for microphysiological modeling of fibrotic diseases. *Lab Chip* **2020**, *20* (19), 3601−3611.

(10) Zamprogno, P.; Wüthrich, S.; Achenbach, S.; Thoma, G.; Stucki, J. D.; Hobi, N.; Schneider-Daum, N.; Lehr, C.-M.; Huwer, H.; Geiser, T.; Schmid, R. A.; Guenat, O. T. Second-generation lung-on-a-chip with an array of stretchable alveoli made with a biological membrane. *Commun. Biol.* **2021**, *4* (1), 168.

(11) Montalvo-Parra, M. D.; Ortega-Lara, W.; Loya-García, D.; Bustamante-Arias, A.; Guerrero-Ramírez, G. I.; Calzada-Rodríguez, C. E.; Torres-Guerrero, G. F.; Hernández-Sedas, B.; Cárdenas-Rodríguez, I. T.; Guevara-Quintanilla, S. E.; Salán-Gomez, M.; Hernández-Delgado, M. A.; Garza-González, S.; Gamboa-Quintanilla, M. G.; Villagómez-Valdez, L. G.; Zavala, J.; Valdez-García, J. E. Customizable Collagen Vitrigel Membranes and Preliminary Results in Corneal Engineering. *Polymers* **2022**, *14* (17), 3556.

(12) Puleo, C. M.; McIntosh Ambrose, W.; Takezawa, T.; Elisseeff, J.; Wang, T.-H. Integration and application of vitrified collagen in multilayered microfluidic devices for corneal microtissue culture. *Lab Chip* **2009**, *9* (22), 3221−3227.

(13) Hori, T.; Okae, H.; Shibata, S.; Kobayashi, N.; Kobayashi, E. H.; Oike, A.; Sekiya, A.; Arima, T.; Kaji, H. Trophoblast stem cell-based organoid models of the human placental barrier. *Nat. Commun.* **2024**, *15* (1), 962.

(14) Lee, J. S.; Romero, R.; Han, Y. M.; Kim, H. C.; Kim, C. J.; Hong, J. S.; Huh, D. Placenta-on-a-chip: a novel platform to study the biology of the human placenta. *J. Matern Fetal Neonatal Med.* **2016**, *29* (7), 1046−1054.

(15) Kim, J.; Kong, J. S.; Kim, H.; Jo, Y.; Cho, D.-W.; Jang, J. A Bioprinted Bruch's Membrane for Modeling Smoke-Induced Retinal Pigment Epithelium Degeneration via Hybrid Membrane Printing Technology. *Adv. Healthcare Mater.* **2022**, *11* (24), 2200728.

(16) Arık, Y. B.; de sa Vivas, A.; Laarveld, D.; van Laar, N.; Gemser, J.; Visscher, T.; van den Berg, A.; Passier, R.; van der Meer, A. D. Collagen I Based Enzymatically Degradable Membranes for Organ-on-a-Chip Barrier Models. *ACS Biomater. Sci. Eng.* **2021**, *7* (7), 2998−3005.

(17) Wang, X.; Maruotti, J.; Majumdar, S.; Roman, J.; Mao, H.-Q.; Zack, D. J.; Elisseeff, J. H. Collagen vitrigels with low-fibril density enhance human embryonic stem cell-derived retinal pigment

https://doi.org/10.1021/acsbiomaterials.4c01112
ACS Biomater. Sci. Eng. 2024, 10, 5653−5665

epithelial cell maturation. *J. Tissue Eng. Regen. Med.* **2018**, *12* (3), 821−829.
(18) Bacakova, M.; Pajorova, J.; Stranska, D.; Hadraba, D.; Lopot, F.; Riedel, T.; Brynda, E.; Zaloudkova, M.; Bacakova, L. Protein nanocoatings on synthetic polymeric nanofibrous membranes designed as carriers for skin cells. *Int. J. Nanomed.* **2017**, *12*, 1143−1160.
(19) Gilbert, D. L.; Okano, T.; Miyata, T.; Kim, S. W. Macromolecular diffusion through collagen membranes. *Int. J. Pharm.* **1988**, *47* (1−3), 79−88.
(20) Fields, M. A.; Del Priore, L. V.; Adelman, R. A.; Rizzolo, L. J. Interactions of the choroid, Bruch's membrane, retinal pigment epithelium, and neurosensory retina collaborate to form the outer blood-retinal-barrier. *Prog. Retin. Eye Res.* **2020**, *76*, 100803.
(21) Lidgerwood, G. E.; Senabouth, A.; Smith-Anttila, C. J. A.; Gnanasambandapillai, V.; Kaczorowski, D. C.; Amann-Zalcenstein, D.; Fletcher, E. L.; Naik, S. H.; Hewitt, A. W.; Powell, J. E.; Pébay, A. Transcriptomic Profiling of Human Pluripotent Stem Cell-derived Retinal Pigment Epithelium over Time. *Genomics, Proteomics Bioinf.* **2021**, *19* (2), 223−242.
(22) Wang, H.; Ninomiya, Y.; Sugino, I. K.; Zarbin, M. A. Retinal Pigment Epithelium Wound Healing in Human Bruch's Membrane Explants. *Invest. Ophthalmol. Vis. Sci.* **2003**, *44* (5), 2199−2210.
(23) Curcio, C. A.; Johnson, M. Structure, function, and pathology of Bruch's membrane. *Retina*; Elsevier Inc., 2013; Vol. *1*, pp 466−481.
(24) Ramrattan, R. S.; van der Schaft, T. L.; Mooy, C. M.; de Bruijn, W. C.; Mulder, P. G.; de Jong, P. T. Morphometric analysis of Bruch's membrane, the choriocapillaris, and the choroid in aging. *Invest. Ophthalmol. Vis. Sci.* **1994**, *35* (6), 2857−2864.
(25) Newton, J. D.; Song, Y.; Park, S.; Kanagarajah, K. R.; Wong, A. P.; Young, E. W. K. Tunable In Situ Synthesis of Ultrathin Extracellular Matrix-Derived Membranes in Organ-on-a-Chip Devices. *Adv. Healthcare Mater.* **2024**, *13*, No. e2401158.
(26) Booij, J. C.; Baas, D. C.; Beisekeeva, J.; Gorgels, T. G. M. F.; Bergen, A. A. B. The dynamic nature of Bruch's membrane. *Prog. Retin. Eye Res.* **2010**, *29* (1), 1−18.
(27) Ferrara, M.; Lugano, G.; Sandinha, M. T.; Kearns, V. R.; Geraghty, B.; Steel, D. H. W. Biomechanical properties of retina and choroid: a comprehensive review of techniques and translational relevance. *Eye* **2021**, *35* (7), 1818−1832.
(28) Wang, X.; Teoh, C. K. G.; Chan, A. S. Y.; Thangarajoo, S.; Jonas, J. B.; Girard, M. J. A. Biomechanical Properties of Bruch's Membrane-Choroid Complex and Their Influence on Optic Nerve Head Biomechanics. *Invest. Ophthalmol. Vis. Sci.* **2018**, *59* (7), 2808−2817.
(29) Bürzle, W.; Mazza, E.; Moore, J. J. About puncture testing applied for mechanical characterization of fetal membranes. *J. Biomech. Eng.* **2014**, *136* (11), 111009.
(30) *Transwell (R) Permeable Supports; CLS-CC-011REV4*, 2007.
(31) Hussain, A. A.; Starita, C.; Hodgetts, A.; Marshall, J. Macromolecular diffusion characteristics of ageing human Bruch's membrane: Implications for age-related macular degeneration (AMD). *Exp. Eye Res.* **2010**, *90* (6), 703−710.
(32) Moore, D. J.; Clover, G. M. The Effect of Age on the Macromolecular Permeability of Human Bruch's Membrane. *Invest. Ophthalmol. Vis. Sci.* **2001**, *42* (12), 2970−2975.
(33) Galloway, C. A.; Dalvi, S.; Shadforth, A. M. A.; Suzuki, S.; Wilson, M.; Kuai, D.; Hashim, A.; MacDonald, L. A.; Gamm, D. M.; Harkin, D. G.; Singh, R. Characterization of Human iPSC-RPE on a Prosthetic Bruch's Membrane Manufactured From Silk Fibroin. *Invest. Ophthalmol. Vis. Sci.* **2018**, *59* (7), 2792−2800.
(34) Sugino, I. K.; Rapista, A.; Sun, Q.; Wang, J.; Nunes, C. F.; Cheewatrakoolpong, N.; Zarbin, M. A. A Method to Enhance Cell Survival on Bruch's Membrane in Eyes Affected by Age and Age-Related Macular Degeneration. *Invest. Ophthalmol. Vis. Sci.* **2011**, *52* (13), 9598−9609.
(35) Paek, J.; Park, S. E.; Lu, Q.; Park, K.-T.; Cho, M.; Oh, J. M.; Kwon, K. W.; Yi, Y.-s.; Song, J. W.; Edelstein, H. I.; Ishibashi, J.; Yang, W.; Myerson, J. W.; Kiseleva, R. Y.; Aprelev, P.; Hood, E. D.; Stambolian, D.; Seale, P.; Muzykantov, V. R.; Huh, D. Microphysiological Engineering of Self-Assembled and Perfusable Microvascular Beds for the Production of Vascularized Three-Dimensional Human Microtissues. *ACS Nano* **2019**, *13* (7), 7627−7643.
(36) Dunn, K. C.; Aotaki-Keen, A. E.; Putkey, F. R.; Hjelmeland, L. M. ARPE-19, a human retinal pigment epithelial cell line with differentiated properties. *Exp. Eye Res.* **1996**, *62* (2), 155−170.
(37) Ablonczy, Z.; Dahrouj, M.; Tang, P. H.; Liu, Y.; Sambamurti, K.; Marmorstein, A. D.; Crosson, C. E. Human retinal pigment epithelium cells as functional models for the RPE in vivo. *Invest. Ophthalmol. Vis. Sci.* **2011**, *52* (12), 8614−8620.
(38) Ribeiro, M.; Pasini, S.; Baratta, R. O.; Del Buono, B. J.; Schlumpf, E.; Calkins, D. J. Collagen Mimetic Peptides Promote Adherence and Migration of ARPE-19 Cells While Reducing Inflammatory and Oxidative Stress. *Int. J. Mol. Sci.* **2022**, *23* (13), 7004.
(39) Chichagova, V.; Hallam, D.; Collin, J.; Buskin, A.; Saretzki, G.; Armstrong, L.; Yu-Wai-Man, P.; Lako, M.; Steel, D. H. Human iPSC disease modelling reveals functional and structural defects in retinal pigment epithelial cells harbouring the m.3243A > G mitochondrial DNA mutation. *Sci. Rep.* **2017**, *7* (1), 12320.

https://doi.org/10.1021/acsbiomaterials.4c01112
ACS Biomater. Sci. Eng. 2024, 10, 5653−5665